Computers, Materials & Continua

Tech Science Press

https://doi.org/10.32604/cmc.2026.076994

ARTICLE

Intention Prediction-Based Automated Vehicle Control Mechanism Using Social-Pooling LSTM and Pass-Through Time Window Optimization

Donghee Oh[1], Chris Lee[2] and Juneyoung Park[1,3,*]

[1]Department of Smart City Engineering, Hanyang University, Ansan, Republic of Korea
[2]Department of Civil & Environmental Engineering, University of Windsor, 401 Sunset Ave, Windsor, ON, Canada
[3]Department of Transportation and Logistics Engineering, Hanyang University, Ansan, Republic of Korea

*Corresponding Author: Juneyoung Park. Email: juneyoung@hanyang.ac.kr

Received: 30 November 2025; Accepted: 01 April 2026; Published: 08 May 2026

ABSTRACT: This study presents a novel integrated framework for autonomous vehicle control at unsignalized intersections in mixed traffic environments, addressing the critical challenge of coordinating Society of Automotive Engineers (SAE) level 4 connected and autonomous vehicles (CAVs) and manually driven vehicles (MVs). The combination of driving intention prediction with a Social Long Short-Term Memory (Social LSTM) and a scheduling algorithm with optimization-driven Pass-through Time Windows (PTWs) is adopted to address traffic flow uncertainty. The Social LSTM model with spatial pooling layers to capture complex multi-vehicle interactions and predict surrounding vehicles' trajectories and maneuver intentions using naturalistic driving data from the CitySim dataset was applied. Unlike conventional approaches that treat prediction and control separately, this framework leverages high-confidence trajectory predictions to inform proactive scheduling decisions for conflict mitigation. The PTW scheduling algorithm formulates intersection management as a constrained optimization problem, dynamically allocating non-overlapping temporal windows for vehicle entering and exiting while considering vehicle dynamics, safety gaps, and deceleration constraints. Comprehensive simulation analysis across varying traffic volumes and CAV market penetration rates reveals significant improvements in both safety and operational efficiency. The scheduling algorithm has notably reduced traffic delay times while maintaining balance with safety measures. This finding provides a fundamental basis for infrastructure-based cooperative driving research, serving as a contributing factor for the development of advanced traffic management systems during the mixed-traffic period.

KEYWORDS: Scheduling algorithm; linear optimization; trajectory prediction; deep learning; social LSTM model; connected and autonomous vehicle

1 Introduction

Recently, the expectation of autonomous driving has led to research and interest in the technology and its potential impact. In 2014, the Society of Automotive Engineers (SAE) published the J3016 standard, which classifies autonomous vehicles (AVs) into six levels according to their level of automation. Based on this, vehicle driving behavior in urban areas and continuous flow according to the level of AVs [1], design and operation methods for dedicated lanes for AVs, technological acceleration through the development of driver assistance systems [2,3], and research on infrastructure-to-vehicle (I2V) and vehicle-to-infrastructure (V2I) communication technologies, various traffic situations that connected and autonomous vehicles (CAVs) may encounter [4] have been studied.

Despite advances in connected automated driving technologies, it is expected that it will take a long time until traffic flow is fully composed of CAVs [5], highlighting the need to consider traffic flow in the transitional phase of mixed traffic situations. Depending on the proportion of CAVs and manually driven vehicles (MVs), mixed traffic can lead to unstable driving behavior and unexpected crashes. According to California Department of Motor Vehicles (CADMV) crash reports from AV companies in the U.S., crashes involving AVs occurred when AVs stopped driving as they were unable to respond [6]. Therefore, current technology needs further improvement through infrastructure communication support in situations that require cognition and judgement. In particular, autonomous driving at unsignalized intersections requires additional attention because there is no traffic controller and the priority of vehicles may vary depending on their arrival times. As drivers at unsignalized intersections tend to reject small gaps and accept large gaps [7], AVs have difficulty with making decisions and navigating uncertain behaviors at unsignalized intersections, which can slow down traffic flow. Thus, this conservative behavior of AVs can reduce the operational efficiency of traffic flow. Moreover, due to the differences in decision-making between MVs and CAVs, it is necessary to prepare for and support different scenarios of mixed traffic and consider collaborative decision-making for complex scenarios [8].

As a proactive safety measure, various algorithmic methods have been developed and their effectiveness was demonstrated by evaluating them using surrogate safety measures (SSMs) [9–12]. Traffic conflicts are defined as drivers taking evasive action to avoid a collision [13], and at unsignalized intersections, deceleration can be applied as an evasive action. While the uncertainty of whether a vehicle will have conflicts decreases as it approaches an intersection, it increases the probability of crashes [14].

The main contribution of this study is to design an infrastructure-based systematic traffic management method at unsignalized intersections for mixed traffic environments where both CAVs and MVs coexist. For this purpose, the study predicts trajectories of surrounding MVs with a Social Long Short-Term Memory (Social LSTM) model using naturalistic driving data. CAVs have the advantage of detecting the position and speed of surrounding vehicles through V2I communication in advance and can react, allowing them to decelerate based on an estimated time of arrival (ETA). CAVs can enter and exit intersections safely and cooperate with a scheduling algorithm. The algorithm prevents overlapping trajectories in conflict zones and minimizes unnecessary stopping maneuvers. As CAVs yield or decelerate according to the situation, the information is shared with roadside units (RSUs). RSUs can optimize sequences to enter an intersection to avoid conflicting vehicle using the Pass-through Time Windows (PTWs) theory.

2 Literature Review

2.1 Vehicle Control Algorithms for Unsignalized Intersections

Previous research has investigated methods for allocating rights of way to prevent vehicle conflicts in mixed traffic conditions at unsignalized intersections. Li et al. [15] constructed a conflict graph to identify potential conflicts between vehicles at unsignalized intersections and assigned optimal priority through a tree search. A heuristic threshold-based motion control (HTMC) strategy was proposed to regulate vehicle acceleration, ensuring that vehicles reached the intersection within the allocated time window. Alanazi & Yi [16] developed a control algorithm that generates additional gaps for the minor road vehicles at unsignalized intersections. By regulating the traffic flow of major road and creating acceptance gaps at the intersection, their method reduced delay times and queue lengths, and improved overall traffic operations and safety at intersections. Zhou et al. [17] introduced differential right-of-way allocation strategies for CAVs, connected human-driven vehicles (CHVs), and MVs at mixed-traffic unsignalized intersections. A real-time control method with a time complexity of O(n) was developed, granting flexible priority to CAVs

while prioritizing human vehicle safety. By classifying CAV control modes into car-following, constant-speed driving, waiting, and conflict resolution, their method reduced average travel time by 5% to 65%. Singh [12] applied SSMs to assess conflict-based safety at unsignalized intersections in India. The study utilized time-to-collision (TTC) and post-encroachment time (PET) as key safety indicators, revealing that T-intersections were safer than Y-intersections and four-way intersections. Providing proper priority and regulating vehicle behavior could improve both operational efficiency and safety. Rachakonda & Pawar [11] evaluated the effectiveness of intersection collision warning systems (ICWS) at unsignalized intersections and identified factors that improved driver behavior, such as reduced reaction time, lower approach speeds, increased critical gap acceptance, and fewer conflicts. Wang et al. [18] applied the time window theory to develop an algorithm that ensures vehicle conflict times at intersections do not overlap. Their optimization model determined the optimal entry time based on spatially linked conflict zones.

2.2 Prediction of Vehicle Trajectory and Driving Intentions at Intersections

The researchers regarded driving intention prediction as a data-driven classification task, focusing on naturalistic driving data and prediction models based on deep learning for predicting a wide range of time series data. Huang et al. [19] proposed the agent selection physical interaction and the linear temporal weights (ASPILin) model to predict trajectories. They used the CitySim dataset for the next 6 s of future trajectory, including 2 s of historical trajectory and the information from up to 4 surrounding vehicles, covering complex urban intersection situations such as unsignalized intersections and roundabouts. Isele et al. [20] predicted trajectory using an analytical and training-free method called Gaussian Lane Keeping that combines a physics-based prediction model with a probabilistic Gaussian model. They predicted trajectories 6 s into the future based on the data from the past 4 s. Alahi et al. [21] introduced Social LSTM, a groundbreaking approach that model interactions between multiple agents in a scene. Social LSTM employs a "social pooling" layer that allows the LSTM networks of nearby agents to share their hidden states, enabling each vehicle to be aware of other vehicles' movements and intentions [22]. The model has demonstrated remarkable improvements in prediction accuracy compared to traditional methods that treat vehicles as independent entities, reducing average prediction error by 23%–45% in dense traffic scenarios.

2.3 Research Gap

The literature review identifies two critical limitations that motivate the present study. First, current approaches often treat drivers' intention prediction and traffic control optimization as separate problems, limiting the potential for seamless cooperation between MVs and CAVs in mixed traffic environments. This separation rarely examines the combined performance of prediction and scheduling. The present study addresses this gap by implementing a stochastic control mechanism where either 100% or 99% of predicted vehicles successfully receive PTWs-based guidance at each 0.1-s control cycle, while 1% experience control dropout and revert to default driving behavior. This approach operationalizes prediction uncertainty through probabilistic control implementation rather than embedding uncertainty distributions within the optimization formulation itself. While maintaining modular independence, this linked approach systematically reveals how prediction reliability thresholds influence priority sequencing and conflict resolution, offering substantive improvements in decision-making visibility. This framework enables proactive control of AV speeds based on the predicted surrounding MVs' maneuver, improving throughput and safety without relying solely on stop-and-wait protocols. Second, unlike prior approaches that apply rigid or heuristic-based scheduling at unsignalized intersections, this study introduces a novel, optimization-driven scheduling algorithm. This approach formulates the conflict resolution and acceptance sequencing problem as a constrained optimization, dynamically assigning non-conflicting entering and exiting time windows to

each vehicle based on their real-time estimated arrival and trajectory predictions. The optimization explicitly considers real-world constraints ensuring both efficiency and safety. By transferring high-confidence intention prediction and solving the vehicle scheduling problem in a principled way, the framework minimizes unnecessary stops and delays while preventing conflicts with surrounding vehicles.

3 Methodology

This study predicts the trajectories of six surrounding vehicles alongside the ego vehicle, totaling seven vehicles, based on their driving intentions using the modeling process which consists of four steps as shown in Fig. 1. First, driving intentions are classified into straight, left-turn, right-turn maneuver identified by heading and course. Second, trajectories are predicted using the deep neural network learning model and the prediction was evaluated with the point-based error metrics. Third, a scheduling algorithm is developed by PTWs information. The entering sequence of all vehicles in the network was determined through an optimization algorithm based on the arrival times of path overlapped vehicles. Lastly, the scheduling algorithm was evaluated with quantitative metrics using SSMs. The algorithm aims at preventing conflicts and improving the overall traffic efficiency at the intersection by controlling the speed of vehicles.

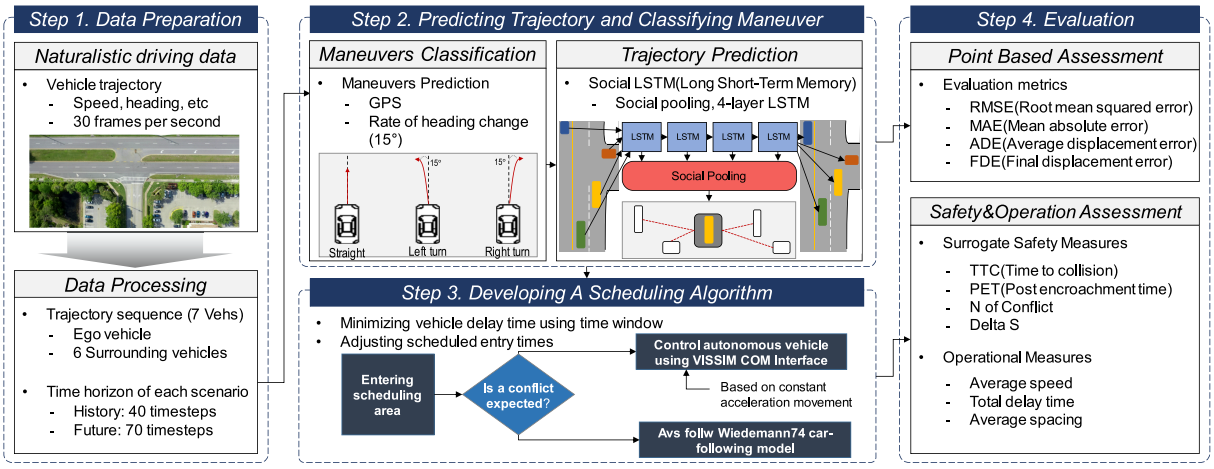

Figure 1: Modelling process for prediction of vehicle trajectory and driving intentions, and traffic optimization at unsignalized intersections.

3.1 Classifying Driver's Maneuver

The Intersection B dataset from CitySim [23] was utilized, which recorded vehicle trajectories at a three-leg unsignalized intersection at a high temporal resolution of 30 frames per second. The dataset includes seven key features including latitude, longitude, speed, heading, length, width, and course. For each scenario, the trajectories of the seven vehicles were captured, providing a comprehensive view of the traffic environment. Data features such as speed and heading have been utilized to predict the vehicle's trajectory and intent in the past studies [24–29].

To process low-noise and accurate prediction of driving intentions, directions such as left-turns, right-turns, and straight-through movements were distinguished. They were classified into target direction based on the vehicle's heading and course information. Surrounding vehicles were grouped according to their relative position on the left-hand side of the major road, right-hand side of the major road, or minor road. A maximum of two vehicles per direction were considered, prioritizing those closest to the ego vehicle. Turning maneuvers were identified by detecting a change in heading greater than 15 degrees, while changes in heading

less than or equal to 15 degrees were categorized as straight movements. To maintain quality of the dataset and exclude irrelevant data such as parked vehicles or sensor noise, vehicles were defined as stationary when they appeared in fewer than 10 frames or had a global positioning system (GPS)-based cumulative displacement of less than 0.0001 degrees in longitude and latitude. Additionally, the scenarios where the ego vehicle exhibited insufficient movement, as indicated by minimal consecutive position changes or limited observation frames, were excluded by classifying all vehicles as stationary and filtering out abnormal or uninformative samples. Applying these criteria, a total of 4500 valid scenarios were generated. The data were split into training and test sets with an 8-to-2 ratio, consisting of 3600 scenarios for training and 900 scenarios for evaluation. For effective modeling, all vehicle coordinates were converted into relative positions with respect to the ego vehicle's latitude and longitude, enabling a consistent frame of reference across scenarios.

3.2 Prediction Model and Evaluation Metrics

3.2.1 Social LSTM

Social LSTM model is a deep learning model designed to predict the future trajectory of each vehicle in a scene where multiple vehicles are driving simultaneously. This model explicitly considers interactions with surrounding vehicles. The model takes relative coordinates as input features, computed relative to the ego vehicle's position at the 40th frame, which serves as the boundary between observation and prediction horizons. This relative coordinate transformation ensures translation invariance and enables the model to learn generalizable spatial interaction patterns regardless of absolute intersection location. The input shape is configured as 40 timesteps by seven vehicles by 2 coordinates for the observation period, and the output shape is 70 timesteps by seven vehicles by 2 coordinates for the prediction period. The vehicle configuration consists of an ego vehicle and 6 neighboring vehicles selected from East, West, and South directions based on proximity. The model collects behavioral information from surrounding vehicles in a special layer called "social pooling" and shares each vehicle's hidden state, allowing each vehicle to consider its interactions with surrounding vehicles.

Unlike the original grid-based social pooling proposed by Alahi et al. [21], this study implemented a distance-based continuous pooling mechanism specifically designed for intersection environments. The distance-based approach calculates the Euclidean distance between all vehicle pairs and applies inverse-distance weighting to aggregate neighboring vehicles' hidden states. Vehicles within a 15-m neighborhood radius are considered for pooling, with closer vehicles receiving higher weights. This continuous pooling approach better captures the variable-density vehicle interactions at unsignalized intersections compared to fixed-grid discretization. This pooled state is added to the input of the next stage of the vehicle, enabling future trajectory predictions that reflect the movements and intentions of surrounding vehicles. The model transforms input features through high-dimensional embedding using dense layers, and then adopts an encoder-decoder structure with multiple LSTM layers. The encoder consists of two LSTM layers that process the observation sequence and capture the temporal dependencies in historical trajectories. Each encoder LSTM layer learns increasingly complex and long-term vehicle movement patterns over time. Early layers understand short-term patterns, such as immediate changes in location and speed, while deeper layers comprehensively understand interactions between vehicles and group behavior. The decoder also consists of two LSTM layers that generate future trajectory predictions based on the encoded representation. The hidden states from the encoder are passed to the decoder as initial states, enabling the model to leverage learned historical patterns for prediction.

At every timestep, the LSTM cell receives pooled hidden-state information from the LSTM cells of neighbors. While pooling the information, the spatial information through grid-based pooling was explained. The hidden state h_i^t of the LSTM at time t captures the latent representation of the i^{th} vehicle in

the scene at that instant [28]. The distance-based social pooling mechanism computes the pooled hidden state H_i^t for vehicle i as shown in Eq. (1):

$$H_i^t = \sum_{j \in N_i} w_{ij} \cdot h_j^{t-1} \tag{1}$$

where h_j^{t-1} is the hidden state of the LSTM corresponding to vehicle j at $t-1$, N_i is the set of neighboring vehicles within the neighborhood radius, and w_{ij} is the inverse-distance weight calculated as shown in Eq. (2):

$$w_{ij} = \left(\frac{\frac{1}{d_{ij}}}{\sum_{k \in N_i} \frac{1}{d_{ik}}} \right) \tag{2}$$

where d_{ij} represents the Euclidean distance between vehicles i and j. This weighting scheme ensures that closer vehicles have greater influence on the pooled representation. The pooled Social hidden-state tensor is embedded into a vector at a_i^t and the coordinates into e_i^t. These embeddings are concatenated and used as the input to the LSTM cell of the corresponding trajectory at time t. This introduces the following recurrence as shown in Eqs. (3)–(5):

$$e_i^t = \varnothing\left(x_t^i, y_t^i; W_e\right) \tag{3}$$

$$a_i^t = \varnothing\left(H_t^i, W_a\right) \tag{4}$$

$$h_i^t = LSTM\left(h_i^{t-1}, e_i^t, a_i^t; W_l\right) \tag{5}$$

where $\varnothing(.)$ is an embedding function with ReLU non-linearlity, and W_e and W_a are embedding weights, respectively. The LSTM weights are denoted by W_l. An important distinction from the traditional LSTM is that the hidden states of multiple LSTMs are coupled by "Social" pooling layer and we jointly back-propagate through multiple LSTMs as shown in Fig. 2.

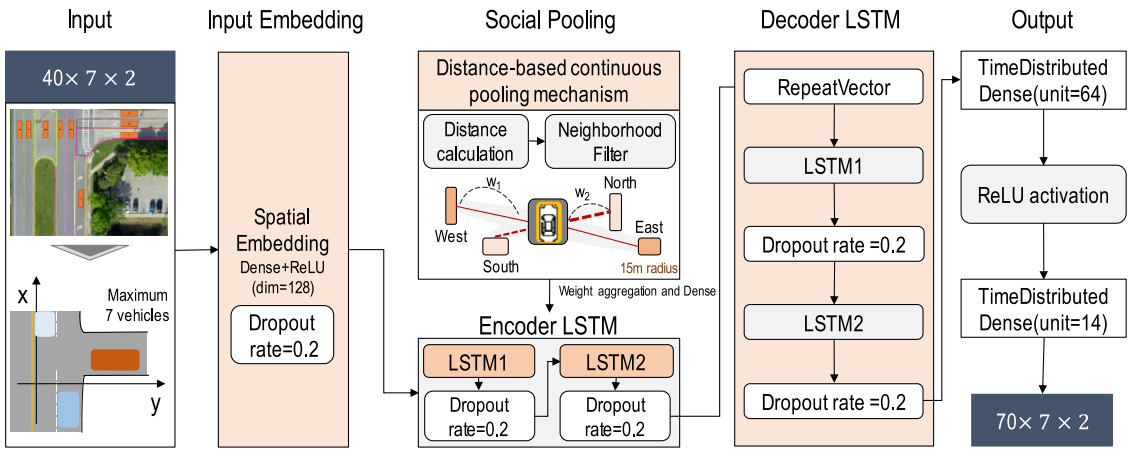

Figure 2: The structure of social LSTM model.

3.2.2 Evaluation Using Point-Based Metrics

The combination of errors provides complementary insights into trajectory prediction performance. While average displacement error (ADE) evaluates the overall accuracy throughout the prediction horizon,

final displacement error (FDE) specifically assesses the endpoint prediction, which is often most critical for decision-making in autonomous driving systems [22]. Models with low ADE but high FDE may perform well in short-term predictions but deteriorate over longer horizons, while models with moderate ADE but low FDE may prioritize accurate endpoint prediction at the expense of path precision. ADE measures the average Euclidean distance between the predicted and ground truth positions over all timesteps of the prediction horizon. FDE measures the Euclidean distance between the predicted and actual positions at the last step of the prediction horizon. ADE and FDE are defined as shown in Eqs. (6) and (7):

$$\text{ADE} = \frac{1}{T}\sum_{t=1}^{T}\sqrt{\left(x_i - x_i^{GT}\right)^2 + \left(y_i - y_i^{GT}\right)^2} \tag{6}$$

$$\text{FDE} = \sqrt{\left(x_T - x_T^{GT}\right)^2 + \left(y_T - y_T^{GT}\right)^2} \tag{7}$$

where T is the prediction horizon (total number of timesteps), $(x_i,\ y_i)$ denotes the predicted trajectory position at timestep i, $(x_T^{GT},\ y_T^{GT})$ denotes the corresponding ground truth position, and the subscript T represents the final timestep. Additionally, mean squared error (MSE), mean absolute error (MAE), and root mean squared error (RMSE) metrics were employed to evaluate the accuracy of trajectory prediction.

3.3 Developing a Scheduling Algorithm by Pass-Through Time Windows (PTWs)

This algorithm aims to minimize traffic conflicts and delays by assigning each vehicle a conflict-free time window based on real-time ETA predictions, surrounding vehicle trajectories, and physical constraints. First, for each entering vehicle at each approach, the ETA at the conflict area and the required passing duration are calculated using predicted trajectories. These are informed by intention-aware models that provide both the possible maneuver and the future trajectory coordinates. Vehicles are grouped by overlapping vehicle static route in the intersection's conflict zones. Vehicles are considered to be in potential conflict and subject to coordinated scheduling if their estimated approach times at the intersection differ by less than 1.5 s and their predicted trajectories spatially overlap within a 100-m radius from the intersection. The choice of a 1.5-s temporal threshold was grounded in traffic safety studies indicating that intervals shorter than this increase conflict risk and reduce safety margins [30]. Similarly, the 100-m spatial boundary represents a practical detection and control range [31], balancing the need for early intervention with computational feasibility, and reflecting the effective communication and sensor detection limits of CAVs in urban environments.

This scheduling algorithm focuses on vehicle pairs within windows and target scenarios where interaction is critical, enabling timely speed adjustment and yielding decisions. Vehicles outside these bounds are managed by standard rules or assumed conflict-free due to temporal-spatial separation. This dual criterion ensures that the PTWs efficiently resolve conflicts only among vehicles whose paths and timing overlap sufficiently to consider safety or operational concerns. The core of the algorithm is to allocate non-overlapping PTWs to each vehicle traversing the same conflict area. For each vehicle, a PTW $[t_{entry}, t_{exit}]$ is determined, where t_{entry} is the scheduled entry time and t_{exit} is the expected exit time from the intersection, calculated based on the vehicle's trajectory and speed profile while considering the minimum safety gap and maximum deceleration constraints.

To implement the scheduling algorithm, the problem is formulated as a constrained optimization that seeks to minimize the total delay introduced by adjusting vehicle entry times while ensuring collision-free traversal within the conflict zone. The optimization model employs three decision variables: the scheduled entry time t_i for vehicle i, the delay offset d_i from the original estimated arrival time t_i, 0, and a binary variable x_{ij} indicating the passing order between conflicting pairs. Key parameters include the traversal time τ_i (computed as connector length divided by maneuver-specific speeds of 17 km/h for left turns, 16 km/h for

right turns, and current speed for straight movements), the safety margin $\Delta = 1.5$ s, the maximum delay cap $d_{i,\max} = 15$ s, and the big-M constant M = 1000 s for disjunctive constraints. The objective function minimizes the sum of all delay offsets as shown in Eq. (8):

$$minimize \sum_{i \in \mathcal{V}} d_i \tag{8}$$

where $\mathcal{V}$ is the set of all vehicles requiring scheduling. Each vehicle i is assigned a PTW $[t^i_{entry,}, t^i_{exit}]$ where t^i_{entry} represents the scheduled entry time, and t^i_{exit} is the expected exit time. The scheduling variables include delay offsets d_i from each vehicle's original estimated time of arrival $t^{(i)}_{entry,0}$ as shown in Eq. (9):

$$t^{(i)}_{entry} = t^{(i)}_{entry,0} + d_i, \qquad d_i \geq 0 \tag{9}$$

The expected exit time from the conflict zone is calculated by adding the traversal time to the scheduled entry time. For each vehicle i, the exit time $t^{(i)}_{exit}$ is defined as shown in Eq. (10):

$$t^{(i)}_{exit} = t^{(i)}_{entry} + \tau_i \tag{10}$$

To prevent collisions, pass-through intervals of conflicting vehicle pairs (i, j) must not overlap, which is enforced by Eq. (11):

$$t^{(i)}_{exit} + \Delta \leq t^{(j)}_{entry} + M(1 - x_{ij}),\ t^{(j)}_{exit} + \Delta \leq t^{(i)}_{entry} + Mx_{ij} \tag{11}$$

where x_{ij} is a binary decision variable indicating the passing order (1 if vehicle i precedes j, 0 otherwise), Δ is the minimum safety gap, and M is a large constant used in the big-M method. Vehicle dynamics are respected by constraining the maximum delay d_i based on feasible deceleration limits ($a_{\max} = -2.0$ m/s^2), ensuring that assigned schedules are physically attainable.

This optimization framework is solved iteratively, employing priorities and conflict structures to determine an optimal or near-optimal scheduling sequence. Once the PTWs are computed, the resulting speed profiles guiding vehicle deceleration and yielding are communicated via the infrastructure to CAVs, enabling smoothness to the assigned schedule. The PTW algorithm is formulated using Mixed-Integer Linear Programming (MILP) and solved using the PuLP and COIN-OR CBC solvers. In the event of a combinatorial explosion, this study filters out all but the potential collision pairs, thereby reducing the size of the problem and capping the maximum delay time at 15 s. If all other methods fail, a fallback using the existing vehicle priority is implemented. For 18 vehicles, the model achieved a maximum of 73.9 ms, meeting the 0.1-s control cycle requirement, demonstrating the feasibility of real-time RSU implementation. The Monte Carlo approach captures system-level reliability degradation without requiring probabilistic formulations within the deterministic MILP solver, thereby maintaining computational tractability while representing prediction uncertainty at the simulation level. A summary of all model parameters is provided in Table 1.

3.4 Test Scenarios and Simulation Environment

The simulation network replicates an unsignalized three-leg urban intersection such as Intersection B, including detailed geometric and operational characteristics such as the number of lanes and entry patterns of turning vehicles. Test scenarios were developed by varying traffic volumes corresponding to level of service (LOS) from B to D, representing different congestion levels commonly observed in urban roads. The simulation scenarios of different mixed traffic compositions were designed using PTV VISSIM microscopic traffic simulation model with market penetration rates (MPRs) of CAVs ranging from 10% to 90% in increments of 10%. Both CAVs and MVs are composed as passenger cars. Vehicle acceptance to

entry patterns were synthesized based on CitySim dataset. In this paper, the results of every scenario were evaluated with 5 replications [32]. The traffic volume at the unsignalized intersection was set based on the criteria of percentage of major road traffic less than 70% as shown in Table 2a. To evaluate the performance of the proposed algorithm, a series of test scenarios and a detailed simulation environment were designed to reflect realistic traffic conditions at unsignalized intersections in mixed traffic environments.

Table 1: Parameters for PTW optimization algorithm.

Parameter	Symbol	Value	Source/Definition
Safety margin (Temporal threshold)	Δ	1.5 s	Traffic safety [30,31]
Maximum comfortable deceleration	$a_{\max}$	-2.0 m/s^2	Traffic safety [30,31]
Maximum delay cap	$d_{i,\max}$	15 s	Service quality
Big-M constant	M	1000 s	Constraint activation
Spatial control range threshold	–	100 m	RSU cooperation range
Left-turn turning speed	–	17 km/h	Naturalistic driving data
Right-turn turning speed	–	16 km/h	Naturalistic driving data
CBC solver time limit	–	5 s	Real-time requirement
Control cycle period	–	0.1 s	Control frequency

Table 2: Parameters for simulation analysis.

(a) Level of Service (LOS) for Unsignalized Intersection

Level of Service	Intersection Total Traffic Volume			Number of Conflicts per Hour (times/h)
	Percentage of Major Road Traffic < 60%	Percentage of Major Road Traffic < 70%	Percentage of Major Road Traffic ≥ 70%	
A	≤320	≤360	≤400	≤60
B	≤640	≤720	≤800	≤120
C	≤960	≤1080	≤1200	≤180
D	≤1280	≤1440	≤1600	≤240

(b) Car-Following Behavior

Parameter			Vehicle Type	
			MV	AV
Car-following model (Wiedemann 74)	Standstill distance (m)		1.5	0.5
	Headway time (s)		0.9	0.5
Lane change	Min. headway (m)		0.5	0.2
	Safety distance reduction factor (%)		90	30
Driver characteristics	Look ahead distance (m)	Min.	0	0
		Max.	250	500
	Desired speed (km/h)	Lower bound	48	50
		Upper bound	58	50

The car-following behavior of Level 4 CAVs was modeled using the Wiedemann 74 model parameters proposed in Atkins [1]. CAVs' car-following behavior has typically been simulated using the adjusted model parameters in interrupted flow conditions [33]. The proposed framework employs a hybrid control approach for CAV behavior. Under normal driving conditions where no potential conflicts are detected, CAVs follow

the car-following model with calibrated parameters as specified in Table 2b. When the PTW scheduling algorithm identifies potential conflicts, the system activates speed control mode through the VISSIM COM Interface. At each simulation time step of 0.1 s, the algorithm retrieves vehicle states including position, speed, and vehicle type. For CAVs within the control zone, the required deceleration is calculated using constant acceleration kinematics to achieve the assigned entry time at the conflict point. If the scheduling cannot fully resolve a conflict, the vehicle applies maximum deceleration to minimize potential collision severity. Once the vehicle exits the conflict zone, control is released and the vehicle returns to Wiedemann 74-based car-following behavior. MVs remain uncontrolled throughout the simulation and follow the default model, as they cannot receive V2I communications from the RSU. Traffic conflicts were identified using the surrogate safety assessment model (SSAM) with default threshold values of TTC less than 1.5 s and PET less than 5 s.

4 Results

4.1 Predicting Vehicle Trajectory and Driver's Maneuver

The prediction performance of the Social LSTM model as shown in Fig. 3 was quantitatively evaluated using multiple error metrics including MAE, RMSE, ADE, and FDE. The model achieved an MAE of 1.788 m, indicating that the predicted vehicle trajectories were generally close to the ground truth as shown in Table 3a. This result is similar to the previous study [21]. The RMSE of 4.161 m confirms the low dispersion of prediction errors, reflecting good overall accuracy. In terms of trajectory-specific metrics, the ADE was 0.994 m, while the FDE was 1.245 m. MAE and RMSE were computed over all seven vehicles, while ADE and FDE were computed for the ego vehicle. These results demonstrate that the Social LSTM model can accurately capture temporal and spatial dynamics of vehicle motions in complex mixed-traffic intersection environments. The model performance of classifying driving intentions was also assessed based on true labels within the test dataset as shown in Table 3b. This result represents multi-object interaction. Both the quantitative metrics and the qualitative trajectory plots indicate that the Social LSTM model not only predicts vehicle positions with high precision, but also reliably identifies their intended maneuvers.

Figure 3: Illustration of social LSTM model predicting trajectories.

Table 3: Results of trajectory prediction and driving intentions.

(a) Performance Metrics for Trajectory Prediction				
MAE (m)		**RMSE (m)**	**ADE (m)**	**FDE (m)**
1.788		4.161	0.994	1.245
(b) Performance Metrics for Driving Intention Classification				
Intention	**Ground Truth (count)**	**Correct (count)**	**Accuracy (%)**	**Precision (%)**	**Recall (%)**
Straight	267	229	85.8	85.1	85.8
Left-turn	317	293	92.4	94.2	92.4
Right-turn	316	298	94.3	92.8	94.3

4.2 Sensitivity Analysis of Key Parameters

The sensitivity analysis was conducted on two key parameters of the proposed framework as shown in Table 4. Expanding the scheduling area from 50 to 100 m resulted in an increase in TTC from 1.00 to 1.14 s and in PET from 0.91 to 1.35 s, while the number of conflicts decreased from 80 to 76. The speed differential also reduced substantially from 10.23 to 6.65 m/s, indicating smoother acceleration and deceleration profiles. Extending the time window from 1.0 to 2.0 s improved TTC from 1.00 to 1.19 s and PET from 1.04 to 1.37 s, while the speed differential decreased from 7.42 to 6.20 m/s. The number of conflicts remained constant at 76 for both the 2.0 and 1.5 s conditions but increased slightly to 78 under the 1.0 s condition. These findings suggest that a larger time window provides the PTW algorithm with sufficient scheduling flexibility to generate safer and smoother passing sequences. Based on these results, the scheduling area of 100 m and time window of 1.5 s were selected as the default configuration for this study, as this combination demonstrated a balanced performance in terms of both safety and ride comfort.

Table 4: Results of sensitivity analysis on scheduling area and time window parameters.

Parameter	Value	TTC (s)	PET (s)	N of Conflicts	Delta S (m/s)
Scheduling Area Range	100 m	1.14	1.35	76	6.65
	75 m	1.10	1.20	78	8.74
	50 m	1.00	0.91	80	10.23
Time Window Range	2.0 s	1.19	1.37	76	6.20
	1.5 s	1.14	1.35	76	6.65
	1.0 s	1.00	1.04	78	7.42

4.3 Statistical Validation

In this study, 'LOS C' was selected as the representative scenario for statistical validation among various level-of-service conditions. For this condition, the results are presented as mean and standard deviation in Table 5. The proposed framework maintained TTC within a relatively stable range of 1.05 to 1.31 s, ensuring consistent safety margins regardless of CAV penetration rate variations. Notably, at 90% CAV penetration, the proposed method achieved a TTC of 1.05 s, representing a 98.1% improvement compared to the baseline value of 0.53 s. At 60% MPR, conflicts were reduced from 96 to 88, corresponding to an 8.3% decrease, while at 90% MPR, conflicts decreased from 60 to 52, a 13.3% reduction. Regarding the speed differential, the

baseline scenario exhibited a sharp increase from 5.13 to 10.35 m/s as CAV penetration increased, whereas the proposed method maintained stable values ranging from 5.51 to 6.65 m/s, demonstrating effective suppression of abrupt acceleration and deceleration maneuvers.

Table 5: Statistical summary of safety metrics under LOS C with scheduling algorithm.

MPR	Baseline Results				Proposed Framework Results			
	TTC (s)	PET (s)	N of Conflicts	Delta S (m/s)	TTC (s)	PET (s)	N of Conflicts	Delta S (m/s)
10%	1.38 ± 0.05	2.31 ± 0.78	48 ± 1.5	5.13 ± 0.54	1.31 ± 0.04	2.54 ± 0.73	52 ± 1.2	5.58 ± 0.34
20%	1.43 ± 0.08	2.23 ± 0.67	84 ± 1.2	4.71 ± 1.13	1.28 ± 0.04	2.01 ± 0.47	88 ± 1.4	6.62 ± 0.89
30%	1.26 ± 0.26	1.46 ± 0.84	80 ± 1.8	5.01 ± 1.83	1.18 ± 0.07	1.89 ± 0.89	76 ± 1.7	5.96 ± 1.39
40%	1.16 ± 0.27	1.27 ± 0.38	88 ± 1.0	6.06 ± 1.35	1.19 ± 0.09	1.60 ± 0.52	80 ± 1.2	5.67 ± 1.88
50%	1.14 ± 0.28	1.24 ± 0.20	80 ± 0.8	6.52 ± 1.30	1.14 ± 0.04	1.35 ± 0.57	76 ± 1.2	6.65 ± 1.05
60%	1.13 ± 0.22	1.34 ± 0.43	96 ± 1.1	7.63 ± 4.91	1.13 ± 0.10	1.62 ± 0.80	88 ± 1.8	5.41 ± 1.93
70%	0.94 ± 0.48	1.30 ± 0.75	92 ± 1.5	7.51 ± 9.57	0.99 ± 0.08	1.29 ± 0.47	80 ± 2.4	6.43 ± 3.86
80%	0.98 ± 0.15	1.65 ± 0.73	74 ± 1.0	8.62 ± 7.85	1.06 ± 0.22	1.38 ± 0.10	60 ± 0.6	6.02 ± 8.69
90%	0.53 ± 0.32	0.67 ± 0.64	60 ± 0.5	10.35 ± 6.66	1.05 ± 0.04	1.15 ± 0.52	52 ± 0.6	5.51 ± 1.54

4.4 Safety Performance of the Scheduling Algorithm

The effects of the scheduling algorithm on safety were compared among different LOS as shown in Table 6 and Fig. 4. In LOS B, the algorithm generally reduced the number of conflicts, with reductions of up to 30% observed at higher MPRs such as 70% and 80%. TTC showed stable or slightly increasing trends in the algorithm condition compared to the no-algorithm condition, with TTC doubling from 0.49 to 0.98 s at 80% MPR. PET also showed a similar trend, although slight decreases were observed at some MPRs. Delta S significantly decreased by up to 55% at 80% MPR, suggesting smoother speed transitions between vehicles under algorithm control. Overall, the proposed scheduling algorithm improved safety in LOS B by reducing the number of conflicts while maintaining or increasing TTC and PET values. In LOS C, the algorithm achieved more pronounced improvements due to increased traffic interactions at this service level. The number of conflicts decreased by 8% to 13% across high MPR scenarios, and Delta S decreased by up to 47% at 90% MPR, indicating effective suppression of abrupt speed changes. The five repeated simulations confirmed consistent performance with acceptable standard deviations, demonstrating the robustness of the proposed framework under moderate congestion conditions. In LOS D, the algorithm maintained its effectiveness despite high-congestion conditions. TTC increased by up to 29% at 80% MPR, demonstrating positive effects of the algorithm in maintaining appropriate gaps between vehicles. The number of conflicts decreased by 10% to 12% at higher penetration rates, and Delta S showed an overall decreasing trend of up to 47%. However, TTC and PET values exhibited greater variability compared to lower congestion levels, indicating that further refinements may be required for extreme traffic conditions. The comparison between 100% and 99% confidence thresholds revealed the tradeoff between prediction reliability and control conservativeness. The 99% threshold, which accounts for trajectory prediction uncertainty, produced comparable safety performance with slightly more conservative scheduling decisions. In LOS C at 90% MPR, the 99% threshold achieved TTC and conflict reduction rates within 7% of the 100% threshold results.

Table 6: Safety performance with and without scheduling algorithm.

LOS B												
MPR (%)	Without Scheduling Algorithm				With Scheduling Algorithm (100%)				With Scheduling Algorithm (99%)			
	TTC (s)	PET (s)	N of Conflicts	Delta S (m/s)	TTC (s)	PET (s)	N of Conflicts	Delta S (m/s)	TTC (s)	PET (s)	N of Conflicts	Delta S (m/s)
10	1.37	2.30	12	5.31	1.37	2.30	12	5.32	1.37	2.30	12	5.32
20	0.90	1.60	20	10.01	1.24	1.82	20	6.10	1.24	1.94	20	6.15
30	1.46	2.67	22	4.91	1.13	1.27	28	5.78	0.93	1.36	28	5.82
40	0.75	1.17	34	4.31	1.07	1.17	24	5.31	1.07	1.38	24	4.94
50	0.75	1.15	28	4.31	1.05	1.13	24	4.91	1.05	1.35	24	4.91
60	0.75	1.15	46	4.22	1.03	0.96	40	4.41	0.98	1.32	44	5.00
70	0.55	1.10	40	6.54	0.91	0.82	28	5.22	0.84	1.24	36	5.63
80	0.49	1.03	26	6.89	0.98	0.62	20	3.12	0.94	0.92	22	4.72
90	0.48	1.01	22	7.43	0.95	0.83	16	7.42	0.93	0.97	18	7.17
LOS C												
MPR (%)	Without Scheduling Algorithm				With Scheduling Algorithm (100%)				With Scheduling Algorithm (99%)			
	TTC (s)	PET (s)	N of Conflicts	Delta S (m/s)	TTC (s)	PET (s)	N of Conflicts	Delta S (m/s)	TTC (s)	PET (s)	N of Conflicts	Delta S (m/s)
10	1.38	2.31	48	5.13	1.31	2.54	52	5.58	1.31	2.08	52	5.58
20	1.43	2.23	84	4.71	1.28	2.01	88	6.62	1.26	1.52	92	6.52
30	1.26	1.46	80	5.01	1.18	1.89	76	5.96	1.14	1.48	78	6.25
40	1.16	1.27	88	6.06	1.19	1.60	80	5.67	1.14	1.32	80	5.44
50	1.14	1.24	80	6.52	1.14	1.35	76	6.65	1.05	1.02	78	6.07
60	1.13	1.34	96	7.63	1.13	1.62	88	5.41	1.13	1.12	92	5.80
70	0.94	1.30	92	7.51	0.99	1.29	80	6.43	1.08	0.96	84	5.58
80	0.98	1.65	74	8.62	1.06	1.38	60	6.02	1.05	0.98	68	5.18
90	0.53	0.67	60	10.35	1.05	1.15	52	5.51	0.98	0.94	56	6.45
LOS D												
MPR (%)	Without Scheduling Algorithm				With Scheduling Algorithm (100%)				With Scheduling Algorithm (99%)			
	TTC (s)	PET (s)	N of Conflicts	Delta S (m/s)	TTC (s)	PET (s)	N of Conflicts	Delta S (m/s)	TTC (s)	PET (s)	N of Conflicts	Delta S (m/s)
10	1.38	2.35	96	4.63	1.36	2.23	96	4.39	1.40	2.43	98	4.80
20	1.16	1.74	144	6.49	1.18	1.83	150	6.45	1.18	1.71	156	6.45
30	1.04	1.63	162	5.37	1.08	1.50	168	5.36	1.10	1.52	166	5.20
40	1.08	1.40	140	6.22	0.93	1.08	138	6.14	0.93	1.00	142	6.11
50	1.12	1.10	144	6.14	1.12	1.20	134	5.89	1.03	1.11	136	6.27
60	1.06	1.13	128	7.75	1.09	1.07	114	7.60	1.01	0.91	118	5.57
70	1.00	1.13	118	6.76	1.26	1.18	106	5.12	1.10	1.41	112	4.38
80	1.00	1.01	112	9.37	1.29	1.05	98	4.95	1.13	0.98	98	5.61
90	1.00	0.84	108	7.01	1.02	0.89	88	6.25	0.98	0.94	94	6.97

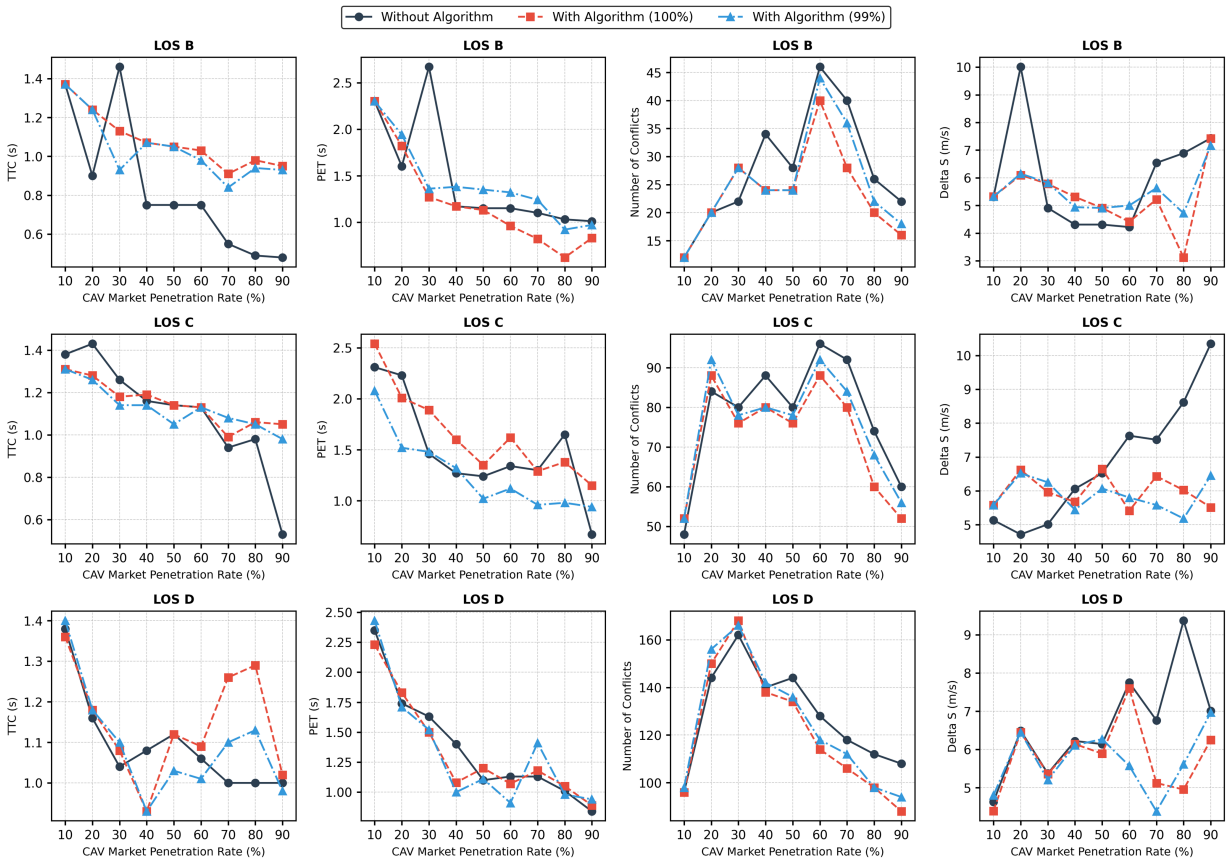

Figure 4: Comparison of SSMs (TTC, PET, N of conflicts, and Delta S) across traffic conditions.

4.5 Operation Performance of the Scheduling Algorithm

The effects of the proposed scheduling algorithm on operational performance were compared among different LOS as shown in Table 7 and Fig. 5. In LOS B, the average speed was similar to the no-algorithm conditions when the scheduling algorithm was applied, remaining stable at approximately 48.7 to 49.7 km/h. The total delay time decreased consistently as MPR increased under both conditions, with the algorithm achieving slightly greater reductions. At 90% MPR, delay time decreased from 29.21 to 22.21 s, representing a 24% reduction. The algorithm reduced delay time and maintained stable distances between vehicles while preserving efficient traffic flow even at high MPR. In LOS C, the average speed remained stable at 48.4 to 49.4 km/h across all conditions. Total delay time showed consistent reductions when the algorithm was applied, with improvements becoming more pronounced at higher MPRs. At 20% MPR, delay time decreased from 249.36 to 190.34 s, and at 90% MPR, it decreased from 136.02 to 124.89 s. The average spacing was longer with the algorithm than the no-algorithm condition at 80% and 90% MPRs, reaching 171 m compared to 154 to 156 m without the algorithm. Overall, in LOS C, the proposed algorithm provided stable speeds in a mixed traffic environment, demonstrating positive effects in mitigating delays and securing distance between vehicles as MPR increases. In LOS D, applying the scheduling algorithm maintained average speed at approximately 47.8 to 48.2 km/h, suggesting that it helped preserve smooth flow even in congested conditions. Total delay time was reduced across all MPR conditions. At 50% MPR, the algorithm reduced total delay time from 288.59 to 255.25 s, representing a 12% reduction. The average spacing consistently increased with the algorithm, improving from 120 to 142 m without the algorithm to 122 to 145 m with the

algorithm. This indicates that the proposed scheduling algorithm can alleviate congestion and secure safe distances effectively even in high-demand traffic conditions.

Table 7: Operation performance with and without scheduling algorithm.

LOS B									
MPR (%)	Without Scheduling Algorithm			With Scheduling Algorithm (100%)			With Scheduling Algorithm (99%)		
	Average Speed (km/h)	Total Delay Time (s)	Average Spacing (m)	Average Speed (km/h)	Total Delay Time (s)	Average Spacing (m)	Average Speed (km/h)	Total Delay Time (s)	Average Spacing (m)
10	49.09	73.20	146.48	48.73	70.51	157.7	48.72	71.13	152.1
20	49.17	67.42	151.17	48.68	64.07	170.85	48.68	64.57	170.68
30	49.25	57.01	155.89	48.75	48.32	162.90	48.72	48.71	159.77
40	49.32	51.62	161.33	48.70	47.69	174.91	48.67	48.36	168.83
50	49.41	42.18	166.25	48.70	40.48	179.45	48.68	40.98	174.51
60	49.46	40.57	171.58	48.71	36.92	184.00	48.70	38.24	175.66
70	49.53	35.23	175.36	48.71	28.2	180.83	48.70	31.79	174.07
80	49.60	31.13	179.75	48.84	24.69	166.18	48.78	30.48	165.94
90	49.65	29.21	185.58	48.75	22.21	178.75	48.75	27.01	178.76
LOS C									
MPR (%)	Without Scheduling Algorithm			With Scheduling Algorithm (100%)			With Scheduling Algorithm (99%)		
	Average Speed (km/h)	Total Delay Time (s)	Average Spacing (m)	Average Speed (km/h)	Total Delay Time (s)	Average Spacing (m)	Average Speed (km/h)	Total Delay Time (s)	Average Spacing (m)
10	48.76	251.89	128.42	48.46	225.04	129.90	48.43	231.31	130.01
20	48.82	249.36	131.66	48.52	190.34	133.44	48.43	228.26	132.23
30	48.88	246.68	134.32	48.48	188.41	135.94	48.46	220.19	135.60
40	48.95	238.15	138.49	48.41	204.77	139.86	48.42	216.27	138.96
50	49.04	216.17	140.65	48.47	198.92	142.42	48.44	207.11	142.02
60	49.16	186.48	146.17	48.01	180.35	145.78	48.62	180.63	145.6
70	49.2	192.04	148.85	48.48	182.47	149.98	48.47	187.12	146.75
80	49.32	159.12	153.71	48.52	151.61	170.96	48.35	157.83	169.87
90	49.41	136.02	156.26	48.56	124.89	170.96	48.26	133.24	169.55
LOS D									
MPR (%)	Without Scheduling Algorithm			With Scheduling Algorithm (100%)			With Scheduling Algorithm (99%)		
	Average Speed (km/h)	Total Delay Time (s)	Average Spacing (m)	Average Speed (km/h)	Total Delay Time (s)	Average Spacing (m)	Average Speed (km/h)	Total Delay Time (s)	Average Spacing (m)
10	48.65	336.10	119.67	47.75	328.80	126.19	47.29	329.53	124.58
20	48.68	357.26	121.66	47.93	332.28	121.82	47.66	342.20	121.45
30	48.76	353.39	123.86	48.03	313.43	124.78	47.92	322.67	124.09
40	48.88	324.61	125.96	48.12	305.12	128.24	48.02	314.35	128.27
50	48.98	288.59	126.86	48.16	255.25	130.57	48.05	271.49	130.35
60	49.15	215.5	131.64	48.18	204.78	134.42	48.09	204.94	134.96
70	49.2	216.13	133.96	48.01	204.37	137.15	48.00	204.43	137.09
80	49.3	193.01	139.54	48.09	190.26	144.60	48.04	192.39	143.76
90	49.38	163.58	141.79	48.18	160.52	144.04	47.58	160.03	142.53

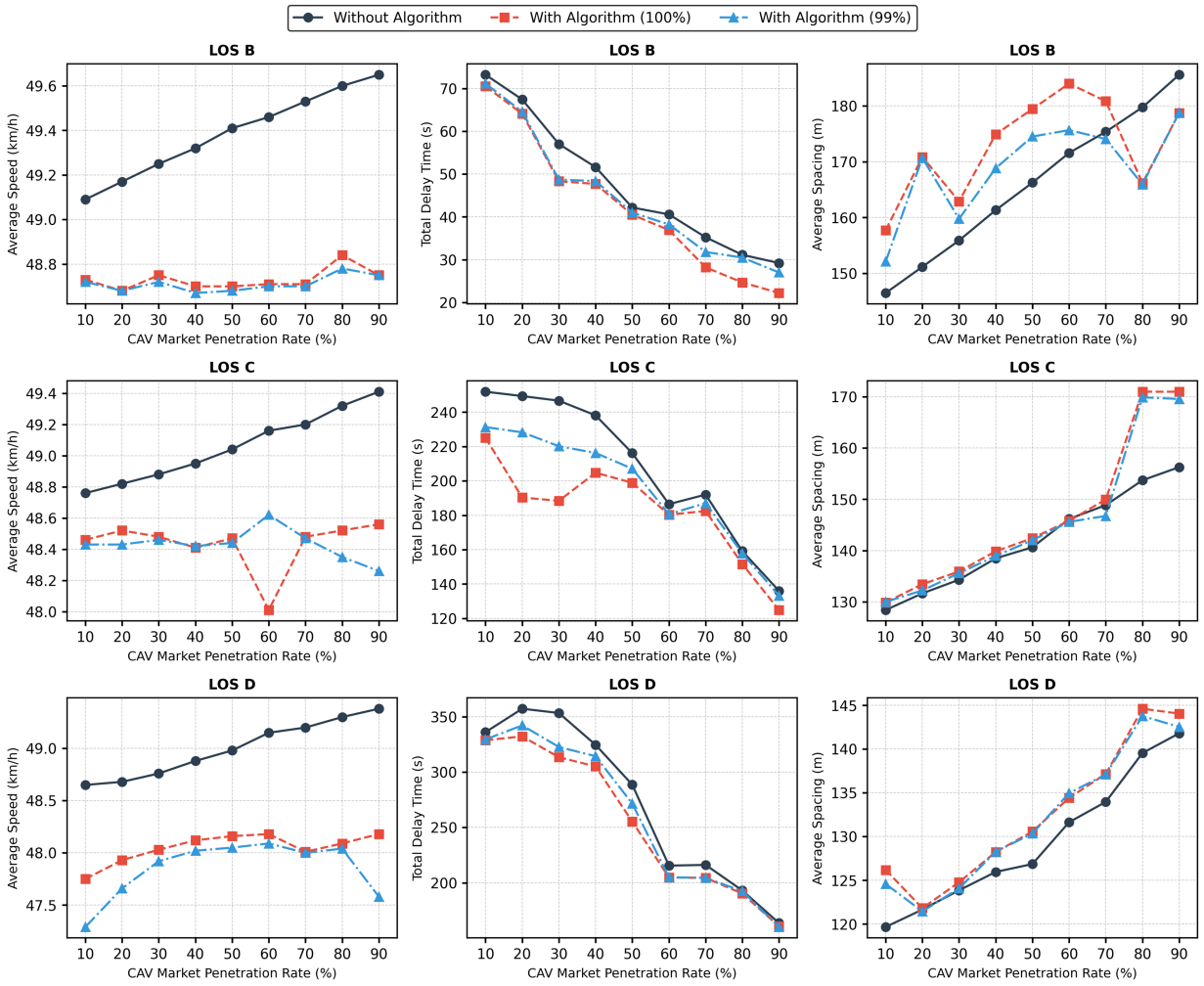

Figure 5: Comparison of operational measures (AVG speed, total delay, AVG spacing) across traffic conditions.

5 Discussions

The demonstrated effectiveness of the Social LSTM-PTW integrated framework represents a significant advancement over existing approaches that treat trajectory prediction and traffic control as separate problems [15,17]. The framework addresses this limitation by seamlessly combining high-confidence intention prediction with optimization-driven scheduling, resulting in more proactive and adaptive conflict resolution. The Social LSTM model's superior prediction accuracy compared to conventional trajectory prediction methods enables more reliable estimation of vehicle arrival times and conflict probabilities. The intention prediction module achieved an average accuracy of 90.8% across all maneuver classes, with accuracies of 0.858, 0.924, and 0.943 for straight, left-turn, and right-turn maneuvers, respectively, together with consistently high precision and recall. This enhanced prediction capability directly translates to more effective scheduling decisions, as demonstrated by the substantial reduction in the number of conflicts and delay times across all tested scenarios. These findings demonstrate how improved prediction capability can be leveraged for practical traffic management applications.

The conflict reduction at high CAV penetration rates achieved by the framework represents a significant breakthrough in intersection safety management. The consistent safety improvements as shown by longer TTC and PET values across varying traffic conditions indicate that the proposed framework maintains

appropriate safety margins while optimizing traffic flow. This addresses a critical gap identified in the previous studies where safety and efficiency objectives often conflict. The delay reductions achieved by the framework, particularly the delay reductions of up to 24% in LOS B and 12% in LOS D under high-congestion scenarios, are consistent with the performance improvements reported in previous studies [17]. The maintained average speeds and increased vehicle spacing indicate that the framework achieved efficiency gains without compromising safety or comfort.

6 Conclusions

This study introduced an integrated framework for traffic management that combines a Social LSTM-based trajectory and driving intention predictions with a PTW scheduling algorithm, explicitly designed for mixed traffic environments consisting of CAVs and MVs at unsignalized intersections. The core contribution lies in the seamless fusion of accurate prediction of vehicle trajectories based on surrounding vehicles' driving intentions with an optimization-driven scheduling strategy that dynamically allocates non-conflicting temporal windows in complex, unsignalized intersections. The Social LSTM model, validated separately on CitySim naturalistic driving data, demonstrated the technical feasibility of achieving high prediction accuracy necessary for proactive traffic management. The simulation results, conducted under the standard microsimulation assumption of perfect trajectory knowledge, represent the performance potential when prediction technologies mature to these demonstrated accuracy levels. This prospective evaluation provides the scheduling algorithm with precise estimated times of arrival and expected passing durations under idealized conditions, thereby underpinning the reliable avoidance of conflicts and enhancement of overall traffic performance.

Simulation results under a wide range of traffic volumes such as LOS B, C, and D and varying MPRs revealed several notable trends. As the proportion of CAVs increased, both surrogate safety measures (TTC, PET, and Delta S) and operational metrics exhibited pronounced improvements at all traffic conditions. Particularly at higher MPRs, the system achieved substantial reductions in both conflict frequency and delay time while increasing average spacing and maintaining stable average speeds. These effects were especially significant under high congestion level where the ability of the optimized scheduling algorithm to adaptively manage growing vehicle densities translates into both higher throughput and robust safety margins. The study further demonstrated that improvements in prediction of trajectory and driving intentions can amplify the benefits of coordinated scheduling, resulting in a synergistic effect as CAV penetration grows. The transition to a higher MPR both empowers the optimization framework to determine vehicle entry more effectively and leverages collaborative vehicle capabilities, thereby reducing reliance on conservative safety buffers traditionally required in manual driving environments. Nevertheless, the study recognizes persistent trade-offs between maximizing operational efficiency and maintaining stringent safety margins. Fluctuations in surrogate safety measures at lower MPRs highlight the need for continuous refinement of scheduling constraints, particularly under mixed traffic scenarios with low CAV adoption. It should be noted that the proposed framework does not require MVs to receive or comply with RSU instructions. MVs are treated as prediction targets only, while control commands are issued exclusively to CAVs.

Real-world deployment will require addressing prediction errors, communication delays, sensor limitations, and potential human driver non-compliance. Additionally, the computational complexity of the PTW optimization increases with the number of vehicles, and the current framework was validated on a three-legged intersection with traffic volume of LOS D. Scalability to larger-scale intersections or higher traffic demands may require distributed optimization approaches or hierarchical control architectures. Future research should focus on incorporating robust optimization formulations with chance constraints that explicitly embed prediction error distributions into the PTW model, implementing adaptive safety

buffers scaled by real-time confidence levels, and validating the proposed framework with empirical field data. While the current stochastic implementation approach prioritizes computational feasibility for real-time deployment, explicit probabilistic optimization would provide more nuanced uncertainty handling for next-generation systems. In summary, the synergy between Social LSTM-based prediction and PTW-based scheduling demonstrates strong potential to fundamentally advance traffic management for unsignalized intersections in mixed traffic. These results underscore the critical value of predictive modeling in traffic coordination and highlight the accelerating benefits of increasing CAV penetration for the realization of safer and more efficient urban mobility.

Acknowledgement: Not applicable.

Funding Statement: This work was supported by the Korea Agency for Infrastructure Technology Advancement (KAIA) grant funded by the Ministry of Land, Infrastructure and Transport (Grant RS-2022-00142565). This work was also supported by National Research Foundation of Korea (NRF) grant funded by the Korea government (MSIT) (No. 2022R1A2C1093424).

Author Contributions: The authors confirm contribution to the paper as follows: Conceptualization, Donghee Oh, Chris Lee and Juneyoung Park; methodology, Donghee Oh, Chris Lee and Juneyoung Park; software, Donghee Oh; validation, Donghee Oh; formal analysis, Donghee Oh; investigation, Donghee Oh and Chris Lee; resources, Donghee Oh; data curation, Donghee Oh; writing—original draft preparation, Donghee Oh and Chris Lee; writing—review and editing, Chris Lee and Juneyoung Park; visualization, Donghee Oh; supervision, Chris Lee and Juneyoung Park; project administration, Juneyoung Park; funding acquisition, Juneyoung Park. All authors reviewed and approved the final version of the manuscript.

Availability of Data and Materials: Not applicable.

Ethics Approval: Not applicable.

Conflicts of Interest: The authors declare no conflicts of interest.

References

1. Atkins. Research on the impacts of connected and autonomous vehicles (CAVs) on traffic flow: summary report. London, UK: Department for Transport; 2016.
2. Li Y, Wang H, Wang W, Xing L, Liu S, Wei X. Evaluation of the impacts of cooperative adaptive cruise control on reducing rear-end collision risks on freeways. Accid Anal Prev. 2017;98:87–95. doi:10.1016/j.aap.2016.09.015.
3. Rana MM, Hossain K. Connected and autonomous vehicles and infrastructures: a literature review. Int J Pavement Res Technol. 2023;16(2):264–84. doi:10.1007/s42947-021-00130-1.
4. Talebpour A, Mahmassani HS. Influence of connected and autonomous vehicles on traffic flow stability and throughput. Transp Res Part C Emerg Technol. 2016;71:143–63. doi:10.1016/j.trc.2016.07.007.
5. Ma L, Qu S, Ren J, Zhang X. Mixed traffic flow of human-driven vehicles and connected autonomous vehicles: string stability and fundamental diagram. Math Biosci Eng. 2023;20(2):2280–95. doi:10.3934/mbe.2023107.
6. Favarò FM, Nader N, Eurich SO, Tripp M, Varadaraju N. Examining accident reports involving autonomous vehicles in California. PLoS One. 2017;12(9):e0184952. doi:10.1371/journal.pone.0184952.
7. Bhatt K, Gore N, Shah J, Arkatkar S. Drivers' dilemma at high-speed unsignalized intersections. Transp Res Rec J Transp Res Board. 2024;2678(3):82–97. doi:10.1177/03611981231178813.
8. Zhong W, Li K, Shi J, Yu J, Luo Y. Reservation-prioritization-based mixed-traffic cooperative control at unsignalized intersections. IEEE Trans Intell Veh. 2024;9(5):4917–30. doi:10.1109/TIV.2024.3370913.
9. Babu SS, Vedagiri P. Proactive safety evaluation of a multilane unsignalized intersection using surrogate measures. Transp Lett. 2018;10(2):104–12. doi:10.1080/19427867.2016.1230172.

10. Paul M, Ghosh I. Development of conflict severity index for safety evaluation of severe crash types at unsignalized intersections under mixed traffic. Saf Sci. 2021;144:105432. doi:10.1016/j.ssci.2021.105432.
11. Rachakonda Y, Pawar DS. Evaluation of intersection conflict warning system at unsignalized intersections: a review. J Traffic Transp Eng Engl Ed. 2023;10(4):530–47. doi:10.1016/j.jtte.2023.04.003.
12. Singh D. Surrogate safety evaluation at uncontrolled intersection in non-lane base traffic conditions. Eur Transp. 2023;(93):1–16. doi:10.48295/et.2023.93.11.
13. Perkins SR, Harris JL. Traffic conflict characteristics—accident potential at intersections. Highw Res Rec. 1968;225:35–43.
14. Ray Sarkar D, Ramachandra Rao K, Chatterjee N. A review of surrogate safety measures on road safety at unsignalized intersections in developing countries. Accid Anal Prev. 2024;195:107380. doi:10.1016/j.aap.2023.107380.
15. Li Y, Liu M, Yang Q, Shen Z, Wu W. Collision-free autonomous scheduling at unsignalized intersection using conflict graph tree search. IEEE Internet Things J. 2024;11(8):14563–78. doi:10.1109/JIOT.2023.3342865.
16. Alanazi F, Yi P. Control logic algorithm to create gaps for mixed traffic: a comprehensive evaluation. Open Eng. 2022;12(1):273–92. doi:10.1515/eng-2022-0035.
17. Zhou J, Shen Z, Wang X, Wang L. Unsignalized intersection management strategy for mixed autonomy traffic streams. IEEE Trans Veh Technol. 2025:1–16. doi:10.1109/TVT.2025.3630320.
18. Wang L, Shi Y, Xiao X, Cao X, Qu F. A scheduling algorithm for pass-through of connected and automated vehicle with different priorities in non-signalized intersection. In: Proceedings of the 2021 IEEE International Conference on Smart Internet of Things (SmartIoT); 2021 Aug 13–15; Jeju Island, Republic of Korea. doi:10.1109/smartiot52359.2021.00034.
19. Huang S, Ye L, Chen M, Luo W, Xu C, Liang D, et al. Enhancing interaction modeling with agent selection and physical methods for trajectory prediction. arXiv:2405.13152v3. 2024.
20. Isele D, Gupta P, Liu X, Bae S. Gaussian lane keeping: a robust prediction baseline. In: Proceedings of the 2024 IEEE 27th International Conference on Intelligent Transportation Systems (ITSC); 2024 Sep 24–27; Edmonton, AB, Canada. doi:10.1109/ITSC58415.2024.10919933.
21. Alahi A, Goel K, Ramanathan V, Robicquet A, Li FF, Savarese S. Social LSTM: human trajectory prediction in crowded spaces. In: Proceedings of the 2016 IEEE Conference on Computer Vision and Pattern Recognition (CVPR); 2016 Jun 27–30; Las Vegas, NV, USA. doi:10.1109/CVPR.2016.110.
22. Benrachou DE, Glaser S, Elhenawy M, Rakotonirainy A. Use of social interaction and intention to improve motion prediction within automated vehicle framework: a review. IEEE Trans Intell Transp Syst. 2022;23(12):22807–37. doi:10.1109/TITS.2022.3207347.
23. Zheng O, Abdel-Aty M, Yue L, Abdelraouf A, Wang Z, Mahmoud N. CitySim: a drone-based vehicle trajectory dataset for safety-oriented research and digital twins. Transp Res Rec. 2024;2678(4):606–21. doi:10.1177/03611981231185768.
24. Klitzke L, Koch C, Koster F. Identification of lane-change maneuvers in real-world drivings with hidden Markov model and dynamic time warping. In: Proceedings of the 2020 IEEE 23rd International Conference on Intelligent Transportation Systems (ITSC); 2020 Sep 20–23; Rhodes, Greece. doi:10.1109/itsc45102.2020.9294481.
25. Leonhardt V, Wanielik G. Recognition of lane change intentions fusing features of driving situation, driver behavior, and vehicle movement by means of neural networks. In: Meyer G, Jakobus C, Müller B, editors. Advanced microsystems for automotive applications 2017. Berlin/Heidelberg, Germany: Springer; 2017. p. 59–69. doi:10.1007/978-3-319-66972-4_6.
26. Li G, Li SE, Liao Y, Wang W, Cheng B, Chen F. Lane change maneuver recognition via vehicle state and driver operation signals—results from naturalistic driving data. In: Proceedings of the 2015 IEEE Intelligent Vehicles Symposium (IV); 2015 Jun 28–Jul 1; Seoul, Republic of Korea. doi:10.1109/ivs.2015.7225793.
27. Li K, Wang X, Xu Y, Wang J. Lane changing intention recognition based on speech recognition models. Transp Res Part C Emerg Technol. 2016;69:497–514. doi:10.1016/j.trc.2015.11.007.
28. Rákos O, Aradi S, Bécsi T. Lane change prediction using gaussian classification, support vector classification and neural network classifiers. Period Polytech Transp Eng. 2020;48(4):327–33. doi:10.3311/pptr.15849.

29. Qu S, Guo F. Behavioral patterns of drivers under signalized and unsignalized urban intersections. Appl Sci. 2024;14(5):1802. doi:10.3390/app14051802.
30. Shou Z, Wang Z, Han K, Liu Y, Tiwari P, Di X. Long-term prediction of lane change maneuver through a multilayer perceptron. In: Proceedings of the 2020 IEEE Intelligent Vehicles Symposium (IV); 2020 Oct 19–Nov 13; Las Vegas, NV, USA. doi:10.1109/iv47402.2020.9304587.
31. Singh D, Das P, Ghosh I. Conflict-Based safety evaluations at unsignalized intersections using surrogate safety measures. Heliyon. 2024;10(5):e27665. doi:10.1016/j.heliyon.2024.e27665.
32. Özkan S, Paldrak M, Öner E. Traffic simulation of a signalized intersection during rush hours: a case study. Endüstri Mühendisliği. 2024;35(2):136–66. doi:10.46465/endustrimuhendisligi.1398935.
33. Kim S, Oh D, Park J. A simulation study for evaluation of autonomous vehicle safety guidance strategies at non-signalized intersection. Int J Highw Eng. 2023;25(6):265–76. doi:10.7855/ijhe.2023.25.6.265.